THE ASTRONOMICAL JOURNAL, 121:2706–2722, 2001 May
© 2001. The American Astronomical Society. All rights reserved. Printed in U.S.A.

THE STRUCTURE OF THE COLD NEUTRAL INTERSTELLAR MEDIUM ON 10–100 AU SCALES

M. D. FAISON[1,2] AND W. M. GOSS[2]

Received 2000 May 16; accepted 2000 October 25

ABSTRACT

We have used the Very Long Baseline Array (VLBA) and the Very Large Array (VLA) to image Galactic neutral hydrogen in absorption toward four compact extragalactic radio sources with a resolution of 10 mas. Previous VLBA data published by Faison et al. have shown the existence of prominent structures in the direction of the extragalactic source 3C 138 with scale sizes of 10–20 AU and changes in H I optical depth in excess of 0.8 ± 0.1. We confirm the small-scale H I optical depth variations toward 3C 147 suggested earlier at a level up to $20\% \pm 5\%$. The sources 3C 119, CJ1 2352+495, and CJ1 0831+557 show no significant change in H I optical depth across the sources with 1 σ limits of 30%, 50%, and 100%. Of the seven sources recently investigated with the VLBA and VLA, only 3C 138 and 3C 147 show statistically significant variations in H I opacities. Deshpande and collaborators have attempted to explain the observed small-scale structures as extensions of the observed power spectra of structures on parsec-size scales. The predictions by Deshpande are consistent with the VLBA H I data observed in the directions of a number of sources, including 3C 147, but they are not consistent with our previous observations of the H I opacity structure toward 3C 138.

Key words: ISM: H I — ISM: structure — techniques: interferometric

1. INTRODUCTION

Structure in the interstellar medium (ISM) is observed on many different size scales, from large, kiloparsec-scale superbubbles (Dewdney & Lozinskaya 1994) to electron density fluctuations in the ionized neutral medium only a few hundred kilometers in size (Armstrong, Rickett, & Spangler 1995). Previous studies have attempted to characterize the structure of the neutral component of the ISM by observing neutral hydrogen in emission over a range of angular scales (e.g., Green 1993; Crovisier & Dickey 1983). These studies have been limited by the angular resolution of single-dish telescopes and connected-element interferometers to size scales from about 0.1 pc to several hundred parsecs. The results of these studies suggested that the neutral ISM is smooth on scales smaller than about 0.1 pc. Because of the typically low brightness temperature of H I in emission on small scales, H I 21 cm emission cannot be detected at milliarcsecond scales using very long baseline interferometry (VLBI) techniques. However, it is possible to image Galactic H I in absorption toward bright extragalactic continuum sources, and thereby to study the structure of the neutral ISM on angular scales from the resolution of the VLBI array (about 5 mas at 21 cm for the Very Long Baseline Array [VLBA]) up to the angular size of the continuum source ($\propto$50 to 200 mas for the sources in this paper). At typical distances to the absorbing gas of 500 to 1000 pc, these angular scales correspond to physical scales of tens to hundreds of AU.

The first VLBI observations of very small scale structure in the neutral ISM were published by Dieter, Welch, & Romney (1976). Observing the source 3C 147 with a single baseline from Hat Creek to the Owens Valley Radio Observatory (150 km), they detected variations in the ratio of the H I absorption line visibility amplitude to the 21 cm continuum visibility amplitude as a function of projected baseline. This change is caused by nonuniform coverage of the H I absorption across the face of the source (Radhakrishnan et al. 1972). Based on the Galactic latitude of the source and on a model of the continuum emission components, they inferred that there was structure in the absorbing H I with a diameter of 70 AU. These results, based on modeling of sparse visibility data, were qualitative, but suggested that there is structure on very small scales in the diffuse neutral ISM.

Subsequent VLBI observations of AU-scale H I structure were published by Diamond et al. (1989). They observed the three extragalactic radio continuum sources 3C 147, 138, and 380 using three large telescopes of the European VLBI Network. The visibility data from the observations were not sufficient to image the sources and the H I absorption distribution. However, the ratio between the line and continuum visibility amplitudes confirmed the nonuniform H I absorption toward 3C 147 observed by Dieter et al. (1976). Large variations toward 3C 138 and moderate variations toward 3C 380 were discovered. Diamond et al. inferred structure in the H I gas with a diameter of 25 AU and densities of (5–10) $\times 10^4$ cm^{-3}, assuming that the line-of-sight dimension is equal to the measured transverse dimension. These conclusions were based on modeling the visibility data rather than on directly imaging the H I optical depth structure.

Confirmation of AU-scale structure in Galactic H I independent of the VLBI data was published by Frail et al. (1994). They observed average variations in the total H I column density of 10%–15% toward nine pulsars at three observing epochs over a period of 1.7 yr. Each pulsar in their study probed a range of physical size scales transverse to the line of sight from 5 to 100 AU. The fact that column density variations over time were observed toward all of the pulsars suggests that AU-scale structure is common throughout the ISM. Also, the fact that Frail et al. observed changes in the total H I column density, but not in the overall line shape, suggests that the AU-scale structure is

[1] Department of Physics and Astronomy, Northwestern University, 2131 Sheridan Road, Evanston, IL 60208; Department of Astronomy, University of Wisconsin at Madison, Madison, WI 53706.
[2] National Radio Astronomy Observatory, P.O. Box O, Socorro, NM 87801.

kinematically related to the diffuse cold neutral medium as a whole.

The first images of AU-scale H I structure in absorption were published by Davis, Diamond, & Goss (1996; hereafter DDG). They used the MERLIN array with five European VLBI Network telescopes to image 3C 147 and 3C 138 in H I optical depth at an angular resolution of 50–150 mas. They observed significant optical depth variations in one of the two H I absorption lines toward both objects. The largest optical depth variation of $\Delta\tau_{\rm H\,I} = 0.16 \pm 0\ .03$ across the source was observed in the 1.3 km s^{-1} absorption line toward 3C 138. A prominent optical depth change of $\Delta\tau_{\rm H\,I} = 0.09 \pm 0.01$ was also observed in the -8 km s^{-1} absorption line toward 3C 147.

There is also evidence for AU-scale structure in the diffuse molecular gas. Moore & Marscher (1995; also Marscher, Moore, & Bania 1993) have discussed changes observed in the column density of H_2CO toward the compact objects 3C 111, BL Lac, and NRAO 150. They observed the three sources over 3.4 yr with the Very Large Array (VLA) in the 6 cm H_2CO line. The motion of the sources due to parallax, as well as the proper motions of the absorbing gas, caused the relative line of sight through the molecular gas to the extragalactic sources to change with time. They observed significant variations in the H_2CO opacities toward 3C 111 and NRAO 150 and inferred structure on linear scales $\sim$10 AU and H_2 densities $\sim 10^6$ cm^{-3}, sizes and densities similar to those observed for the small-scale H I structure.

Heiles (1997) has proposed a geometric model to explain the large variations in column density. This model assumes that the structures are due to filaments or sheets observed edge-on, causing larger variations in column densities over smaller scales to be observed and implying much higher volume densities than are actually present. If the observed structure arises from edge-on sheets, the optical depth images should statistically show smaller scale variations along the axis perpendicular to the sheet compared with variations along the axis parallel with the sheet.

Faison et al. (1998; hereafter FGDT) published high angular resolution (10–20 mas) VLBA images of H I absorption toward 3C 138, QSO 2255+416, and CJ1 0404+768. Pronounced H I optical depth variations were confirmed toward 3C 138, consistent with Diamond et al. (1989) and DDG. Moderate H I variations were observed toward the small angular size source 2255+416, and no significant variations were observed toward 0404+768, suggesting a minimum size for the H I structure of a few tens of AU.

Deshpande, Dwarakanath, & Goss (2000) have evaluated the structure observed in H I absorption toward Cas A over a linear scale of 4 to 0.02 pc. Deshpande (2000) has taken the slope of the power spectrum of fluctuations of $\alpha = -2.75$ and has extrapolated it to scales smaller by 3 orders of magnitude (size scales smaller than 100 AU). Deshpande predicts that optical depth variations as large as 0.1 should be expected on scales of tens of AU. These fluctuations are caused by gradients in the distribution, which are caused in turn by the "red" spectrum (larger scales have more power) of the power spectrum of the H I. The fluctuations observed by the VLBA in the direction of 3C 138 are almost an order of magnitude larger than this prediction. In addition, two-dimensional H I features are observed.

In this paper we present H I optical depth images toward 3C 147, 3C 119, CJ1 2352+495, and CJ1 0831+557, and we discuss our current knowledge of AU-scale structure in the diffuse neutral ISM.

2. OBSERVATIONS AND DATA REDUCTION

FGDT discuss the criteria for selecting sources for imaging in H I absorption with the VLBA. The continuum source must be bright enough at 21 cm to be imaged with acceptable signal-to-noise ratio at sufficient angular and velocity resolution (continuum flux density greater than about 100 mJy beam^{-1} at 5–10 mas resolution). The source must have significant milliarcsecond structure that can be resolved by the VLBA at 21 cm. The source must have significant Galactic H I absorption but not be optically thick ($0.1 < \tau_{\rm H\,I} < 2.0$). The angular resolution of the VLBA at 21 cm is approximately 5 mas. To improve the signal-to-noise ratio in the optical depth cube, we have smoothed the images to an angular resolution of 10 mas. The source 3C 147 was selected based on previous observations of H I small-scale structure. The source 3C 119 was selected as a good candidate for probing small-scale H I based on the H I absorption spectrum toward the source published by Mebold et al. (1981) and on the VLBI continuum images published by Nan et al. (1991). The two sources 0831+557 and 2352+495 were selected from the Caltech-Jodrell Bank survey (Polatidis et al. 1995) based on the VLBI angular structure and on the low Galactic latitude of the sources. Table 1 shows parameters for all four sources.

The basic data reduction procedure is described in FGDT. Each source was observed with all ten VLBA stations and with the phased VLA (as an additional VLBI station) for 12 hr. The data were correlated at the VLBA correlator in Socorro, New Mexico. Four separate interme-

TABLE 1

SOURCE PARAMETERS

Parameter	3C 147	2352+495	3C 119	0831+557
Observed	1998 Oct 22	1998 Oct 12	1998 Sep 21	1997 Sep 11
R.A. (J2000.0)	05 42 36.137881	23 55 09.45816	04 32 36.5030	08 34 54.9040
Decl. (J2000.0)	49 51 07.233596	49 50 08.340230	41 38 28.430	55 34 21.072
Galactic longitude (deg)	161.69	113.71	160.96	162.23
Galactic latitude (deg)	+10.30	−12.03	−4.34	+36.56
Angular resolution (mas)	10	10	10	20
Redshift	0.545	0.237	1.020	0.2412
$S_{21\ \rm cm}$ (Jy)	22.5	2.36	8.60	8.80

NOTE.—Units of right ascension are hours, minutes, and seconds, and units of declination are degrees, arcminutes, and arcseconds.

diate frequencies (IFs) were used, with one IF centered on the absorption lines and three IFs separated by at least 100 km s^{-1} in velocity to sample the 21 cm continuum emission. For all these observations the data were correlated with velocity channels of 0.4 km s^{-1}, and for most of the objects a bandwidth of 500 kHz per IF was used with 256 spectral channels per IF. For the observations of 3C 119 a bandwidth of 1 MHz per IF was used with 512 spectral channels per IF to accommodate the larger velocity range (100 km s^{-1}) of H I absorption components.

All data processing for each object was performed with the AIPS package available from NRAO. The data were amplitudecalibrated and fringe-fitted using standard techniques in AIPS. Once the data were amplitude- and bandpass calibrated, the three continuum IFs were averaged together, self-calibrated, and imaged using the AIPS task IMAGR. The self-calibration phase and amplitude solutions from these continuum images were then applied to the line IF, which was then imaged to produce a total intensity cube as a function of right ascension, declination, and LSR velocity. The velocity channels in this intensity cube that did not show H I absorption were then averaged together to produce a continuum image. This image was used with the intensity cube to produce an H I optical depth cube as a function of right ascension, declination, and LSR velocity. The optical depth cube is calculated as $\tau_{H\,I}(\alpha, \delta, V) = -ln[I_{line}(\alpha, \delta, V)/I_{cont}(\alpha, \delta)]$. Because the signal-to-noise ratio in the optical depth images is poor where the continuum emission is weak, the optical depth images were blanked where the continuum emission was less than 10% of the peak emission. This optical depth cube with dimensions of right ascension, declination, and velocity is the final reduced data for each object.

3. RESULTS

3.1. *3C 147*

The continuum image of 3C 147 is shown in Figure 1. This image was convolved to a resolution of 10 mas. The source is a quasar with a redshift of 0.545 and a total 21 cm flux density of 22.5 Jy. The continuum structure consists of a core component with a broad jet extended to the southwest. Figure 2 shows an H I optical depth spectrum averaged over the entire source. Kalberla, Schwarz, & Goss (1985) deconvolved the H I optical depth spectrum toward 3C 147 into five Gaussian components. In this paper we will

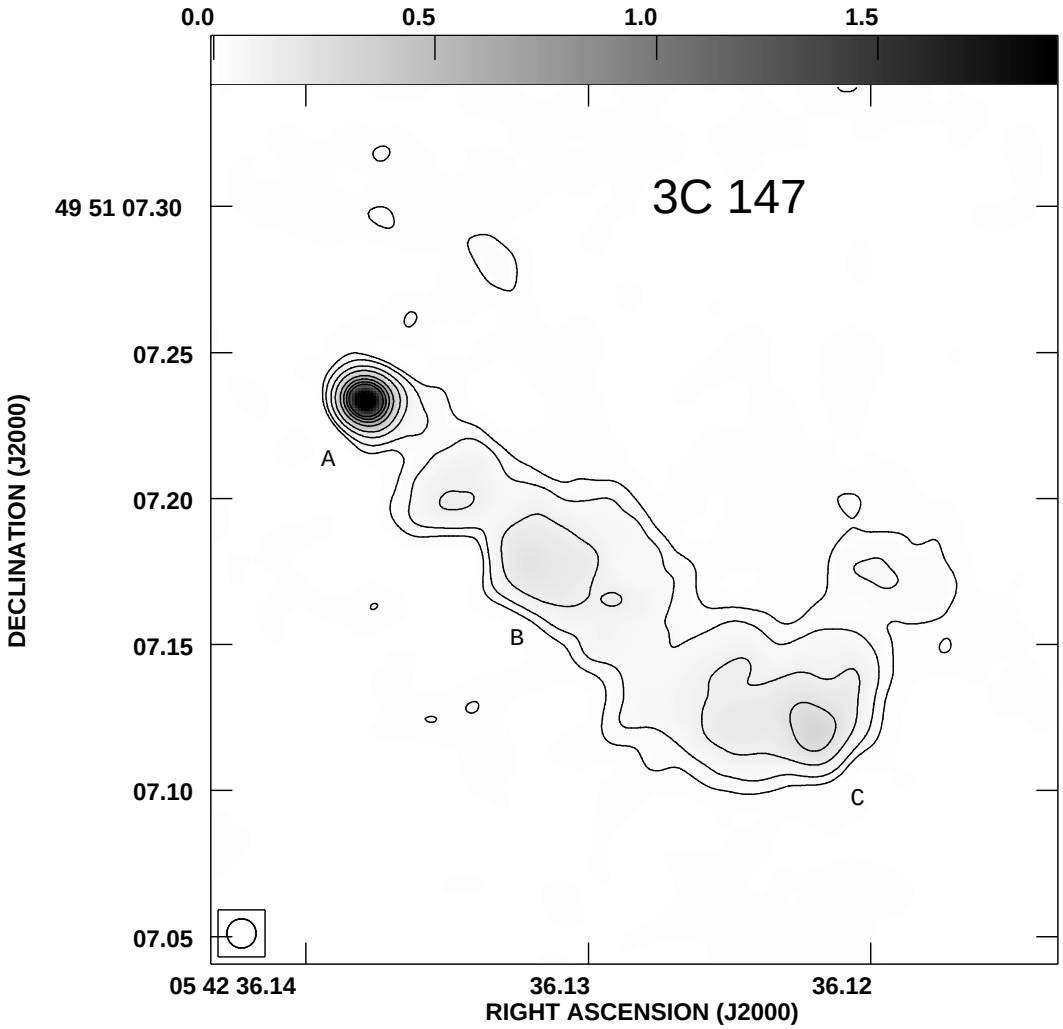


FIG. 1.—Continuum image of 3C 147 at 21 cm obtained with the VLBA and phased VLA. The beam has been convolved to an angular size of 10 mas from an original resolution of 5 × 4 mas. The contours correspond to the continuum emission at 23.1, 46.2, 115, 231, 462, 694, 924, and 1160 mJy $beam^{-1}$.

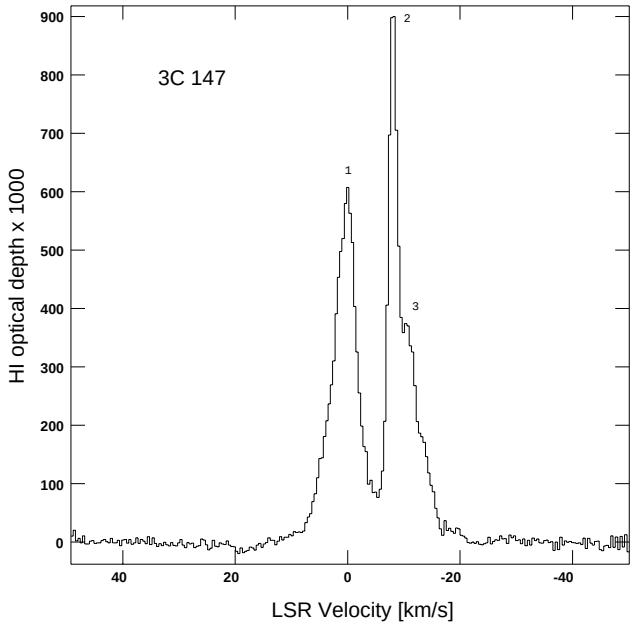


FIG. 2.—H I optical depth spectrum toward 3C 147 averaged over the entire source using the VLBA and phased VLA. The velocity resolution is 0.4 km s^{-1}.

only consider the three components at 0.4, −8.3, and −10.3 km s^{-1}. Figures 3 and 4 show H I optical depth images toward 3C 147 at 0.4 and −8.3 km s^{-1}, respectively. The gray scale indicates H I optical depth from 0 to 1.5 and the contours indicate the low-level continuum emission. Figure 5 shows the 21 cm continuum image with H I optical depth spectra averaged over a beam size of 10 mas toward the three areas of brightest emission (Fig. 1, components labeled "A," "B," and "C"). The dashed line in these plots indicates the averaged spectrum, and the solid line indicates the Gaussian fit produced using the iterative fitting task PROFIT, using the Groningen Image Processing System (GIPSY) package. The parameters of these Gaussian profile fits are given in Table 2.

In the optical depth image at −8.3 km s^{-1} (Fig. 4), there is an increase in optical depth from 0.82 to 1.1 (1 σ is 0.05) between the bright northeast component and the southwest component 190 mas away, consistent with that found by DDG. They observed H I optical depth variations in the −8.3 km s^{-1} absorption line toward 3C 147, but not in the 0.4 km s^{-1} absorption feature.

In the 0.4 km s^{-1} optical depth image (Fig. 3), there is a slight change in optical depth between the two brightest components. The largest optical depth change at this velocity is from 0.5 ± 0.1 to 0.7 ± 0.1 between the bright north-

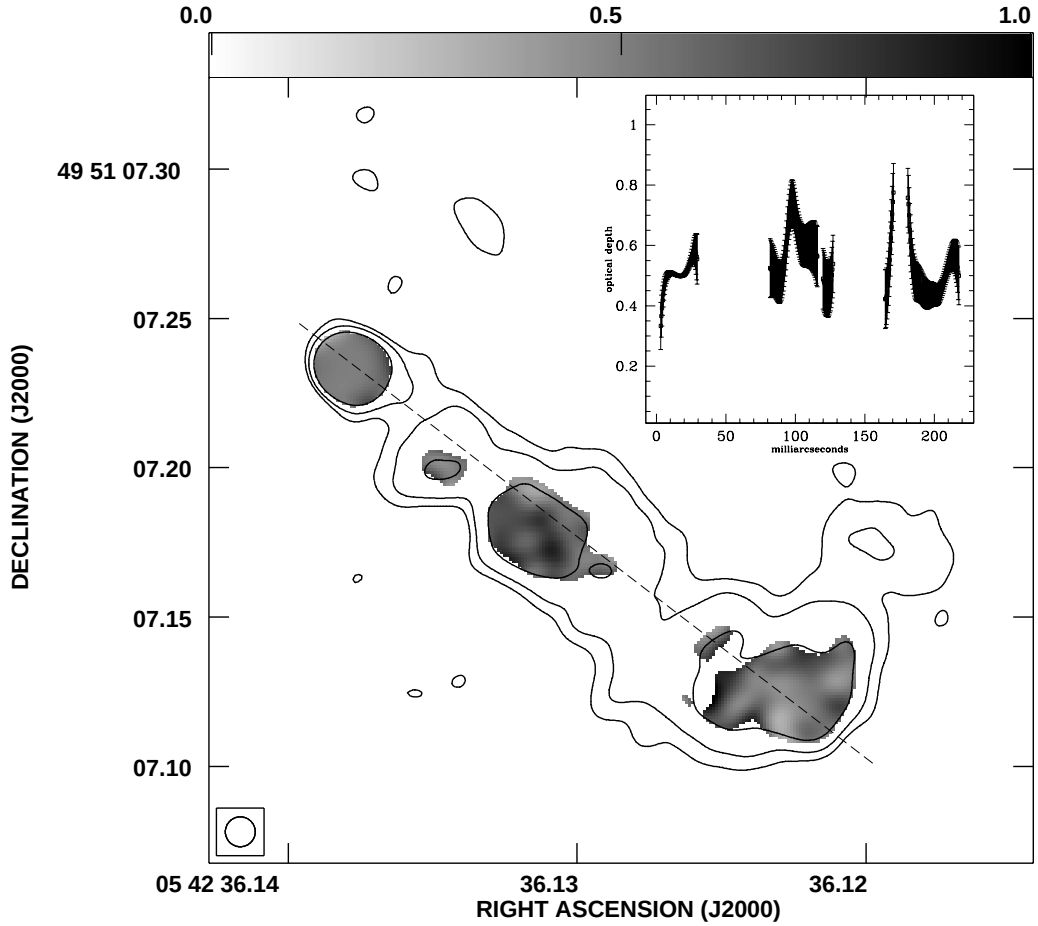


FIG. 3.—H I optical depth image toward 3C 147 in a single 0.4 km s^{-1} velocity channel at 0.4 km s^{-1} (LSR). The angular resolution is 10 mas. The gray scale represents H I optical depth from 0 to 1.0, and the contours represent 21 cm continuum emission at 23.1, 46.2, 116 mJy $beam^{-1}$. The optical depth image has been blanked where the continuum emission is weak (where the error in the optical depth is greater than 0.1). The inset shows a crosscut in optical depth with 2 σ error bars along the axis indicated by the dashed line.

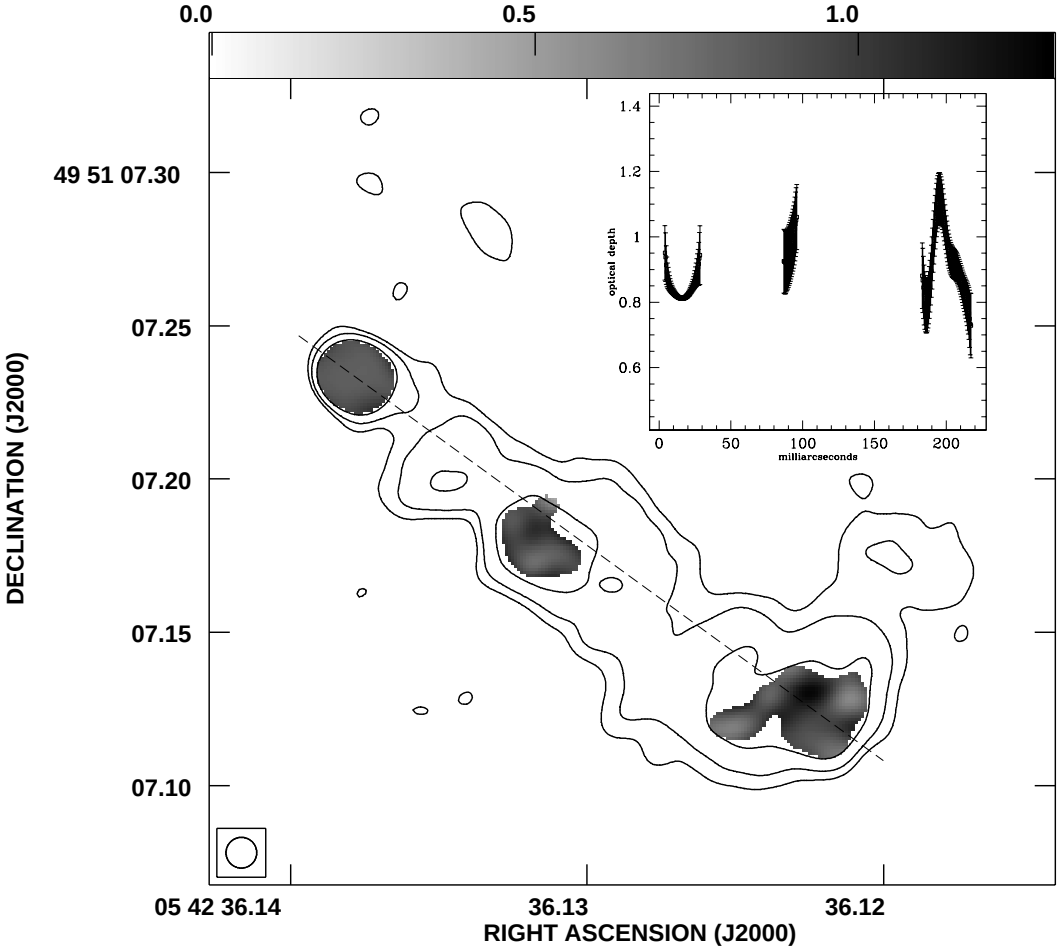


FIG. 4.—H I optical depth image toward 3C 147 in a single 0.4 km s^{-1} velocity channel at -8.3 km s^{-1} (LSR). The angular resolution is 10 mas. The gray scale represents H I optical depth from 0 to 1.3, and the contours represent 21 cm continuum emission at 23.1, 46.2, 116 mJy beam^{-1}. The optical depth image has been blanked where the continuum emission is weak (where the error in the optical depth is greater than 0.1). The inset shows a crosscut with 2 σ error bars in optical depth along the axis indicated by the dashed line.

east component and the component midway along the axis of the source. These are small angular-scale optical-depth variations that would not have been resolved at the 150 mas angular resolution of the MERLIN images published by DDG.

A problem with determining the physical size of this structure is the uncertain determination of the distance to the absorbing H I gas. DDG placed a simple geometric upper limit on the distance to the H I cloud based on the Galactic latitude of the source with $b = +10.^{\circ}3$. Assuming that the cold H I is confined to within 100 pc of the plane, an intervening H I cloud along this line of sight must be within 600 pc of the sun. At a Galactic longitude of 162°, a kinematic distance to the -8.3 km s^{-1} component is uncertain; however, the distance can be estimated at 1.1 kpc using the rotation curve of Fich, Blitz, & Stark (1989). The angular separation between components A and C (see Fig. 1) of 190 mas corresponds to a physical scale of 200 AU at a distance of 1 kpc and 100 AU at 600 pc. The angular separation between components A and B (see Fig. 1) of 83 mas corresponds to 90 AU at 1 kpc and 50 AU at 600 pc. These distances are quite uncertain, and so it is reasonable to approximate the distance to the -8.3 km s^{-1} gas at 1 kpc and the distance to the low-velocity gas at 500 pc.

As with the observations described by FGDT, the circular polarization ($V = \mathrm{RCP} - \mathrm{LCP}$) was imaged for each source, as well as for the total intensity cube. The circular polarization cube can be fitted for Zeeman splitting because of a line-of-sight magnetic field. We fitted the circular polarization spectrum of these sources using the tasks ZEESTAT and ZEESIM in the MIRIAD data analysis package described by Sault, Teuben, & Wright (1995). These tasks average the I and V spectra over the entire source and estimate the leakage of the I spectrum into the V spectrum using an iterative fitting procedure. The strength of the field can be calculated from the V and I spectra as $B_{\|} = 2V/(a\,dI/dv)$, where $a = 2.8$ Hz μG^{-1}. For 3C 147, the fit gives a 2 σ upper limit of 32 μG on the absolute line-of-sight magnetic field averaged over the entire source.

3.2. *3C 119*

The source 3C 119 is a compact symmetric object with a redshift of 0.408 (Nan et al. 1999) and a total flux density of 8.6 Jy. Previous observations of the Galactic H I absorption spectrum toward 3C 119 by Mebold et al. (1981) indicated significant H I absorption along the line of sight. The 21 cm continuum image is shown in Figure 6, convolved to 10 mas angular resolution. Only three bright continuum com-

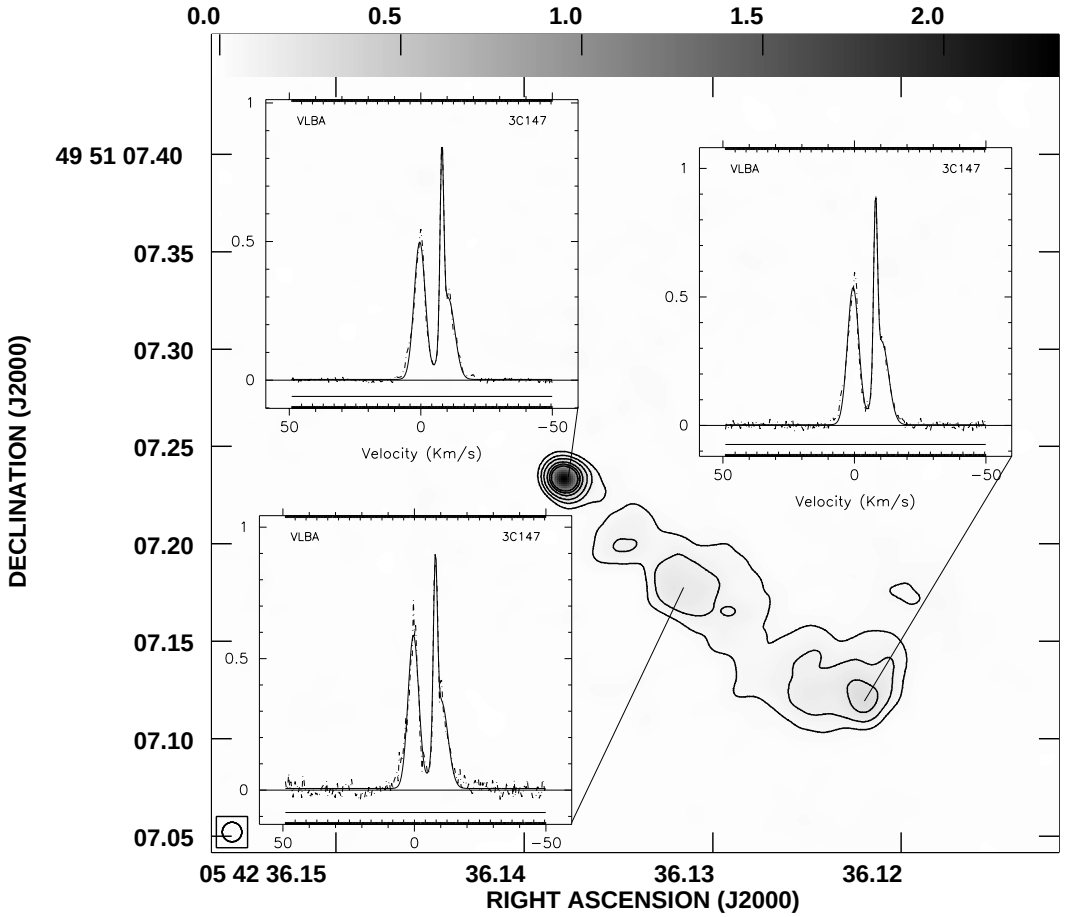


FIG. 5.—Continuum image of 3C 147. Insets show optical depth spectra averaged over the areas of brightest continuum emission. The dashed line in the insets shows the VLBA data, and the solid line indicates the Gaussian component fits. The parameters of the fits are given in Table 2.

ponents are observed in the image, labeled "A," "B," and "C" in Figure 6.

Of the seven sources in the Galactic H I sample, 3C 119 has the lowest Galactic latitude ($b = -4.^{\circ}3$) . This source has a complex H I absorption spectrum with Galactic H I absorption over a velocity range from $+10$ to -63 km s^{-1}. The H I optical depth spectrum toward 3C 119 is shown in Figure 7. Two typical optical depth images for 3C 119 are shown in Figures 8 and 9 for LSR velocities of -4.7 and -62.6 km s^{-1}, respectively. The inset plots show crosscuts from south to north in optical depth through the centers of the two brightest components C and B. The optical depth

TABLE 2

3C 147 H I OPTICAL DEPTH SPECTRUM FIT GAUSSIAN PARAMETERS

Spectral Component	Amplitude (Optical Depth)	Column Density[a] (10^{20} cm^{-2})	Center Velocity (km s^{-1})	Velocity Dispersion (km s^{-1})
Component A:				
1	0.50 ± 0.009	2.44 ± 0.06	0.42 ± 0.03	5.0 ± 0.07
2	0.67 ± 0.03	1.02 ± 0.05	-8.0 ± 0.02	1.6 ± 0.04
3	0.29 ± 0.01	1.72 ± 0.09	-10.3 ± 0.09	6.0 ± 0.1
Component B:				
1	0.58 ± 0.02	2.71 ± 0.14	0.37 ± 0.05	4.7 ± 0.13
2	0.68 ± 0.07	1.15 ± 0.14	-7.9 ± 0.03	1.7 ± 0.1
3	0.33 ± 0.03	1.93 ± 0.2	-10.2 ± 0.2	6.0 ± 0.3
Component C:				
1	0.54 ± 0.01	2.66 ± 0.085	0.49 ± 0.04	5.1 ± 0.09
2	0.69 ± 0.04	1.12 ± 0.08	-8.0 ± 0.02	1.7 ± 0.05
3	0.32 ± 0.02	1.95 ± 0.2	-10.4 ± 0.2	6.2 ± 0.2

[a] Assuming $T_{spin} = 50$ K.

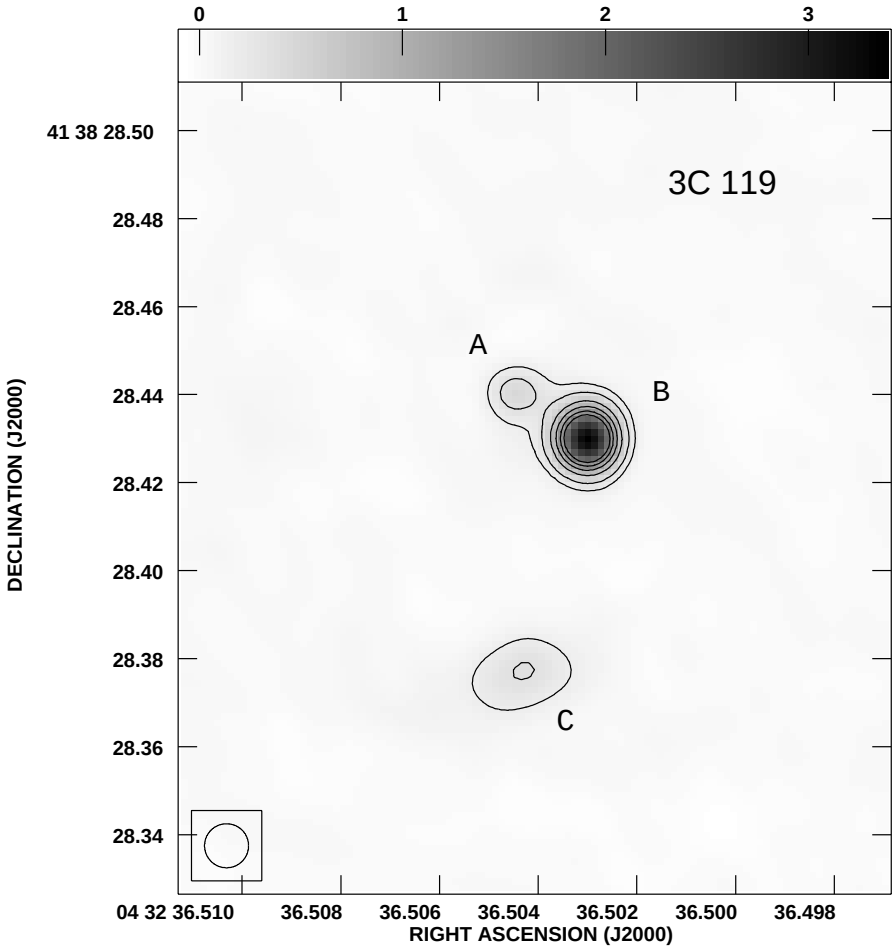


FIG. 6.—Continuum image of 3C 119 at 21 cm from the VLBA and phased VLA. The beam has been convolved to an angular size of 10 mas. The contours represent continuum emission at 169, 337, 674, 1010, 1350, and 1690 mJy beam^{-1}.

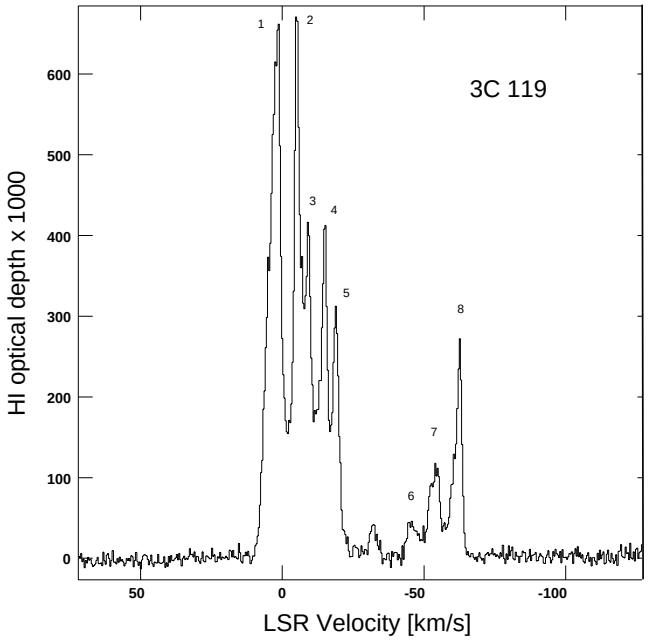


FIG. 7.—H I optical depth spectrum toward 3C 119 averaged over the source. The velocity resolution is 0.4 km s^{-1}. The numbered velocity components are referred to in Table 3.

images at most velocities show no H I optical depth variations between the two components B and C ; the 1 σ upper limit to any change in the opacity is $\Delta\tau \approx 0.2$.

Figure 10 shows the 21 cm continuum image with optical depth spectra toward continuum components B and C, averaged over a beam size of 10 mas. The angular separation of these components is about 53 mas. These two average spectra were fitted with eight Gaussian profiles using PROFIT in the GIPSY data reduction package. The parameters of these two sets of fits are given in Table 3. As in Figure 5 for 3C 147, the dashed lines indicate the data and the solid lines indicate the fits. There is no significant difference in any of the profile fits between the continuum emission components B and C with a 1 σ upper limit of about 10% in column density variation.

The source 3C 119 is at a Galactic longitude of 161°, and a kinematic distance to the H I absorption components cannot be reliably determined so close to the Galactic anticenter. Given the Galactic latitude of the source ($b = -4.^\circ3$), a geometric upper limit on the distance to the H I absorption is 1.3 kpc, again assuming that the H I layer is within 100 pc of the plane. At that distance, the angular resolution in the optical depth images corresponds to a physical size of 13 AU, and the 53 mas separation between components B and C corresponds to 70 AU. The low-velocity absorption

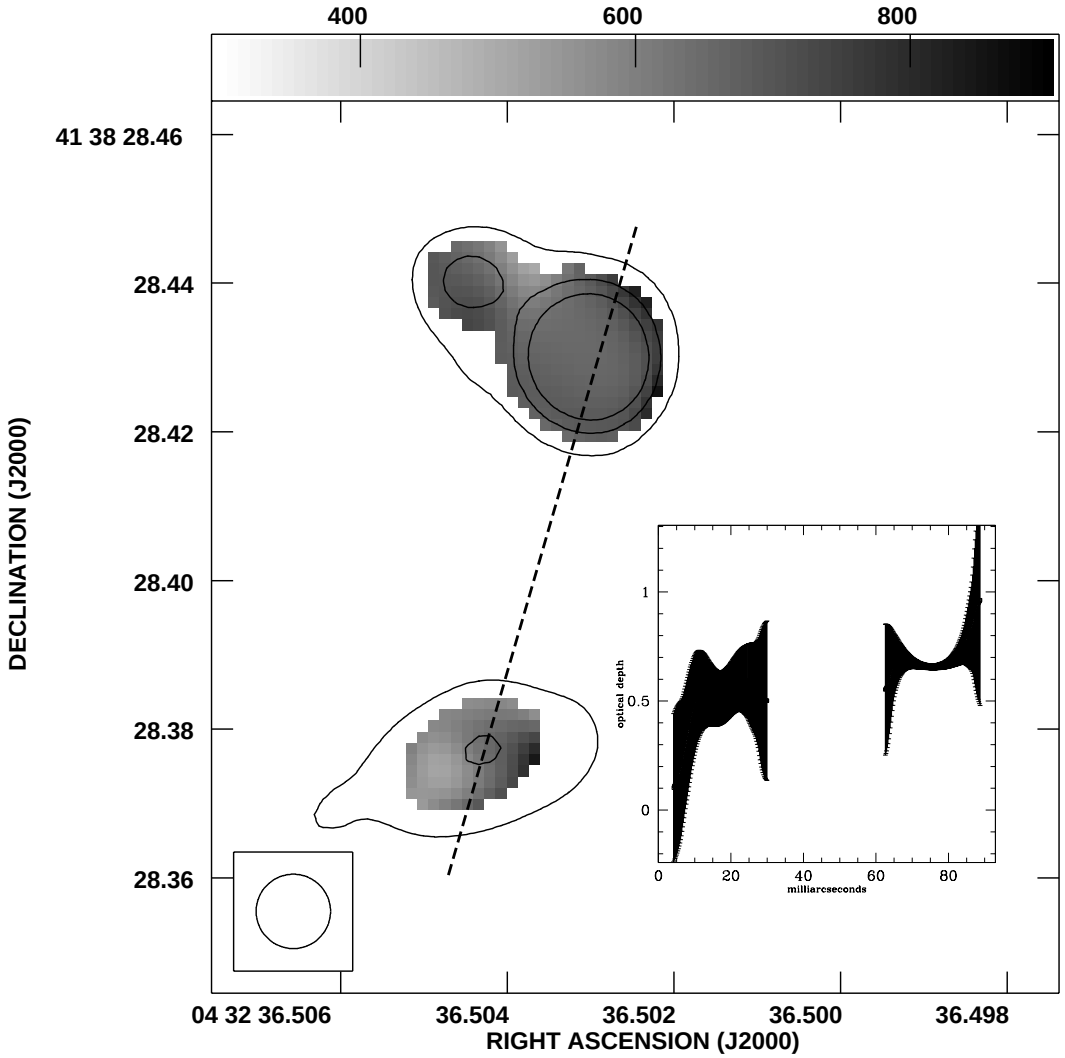


FIG. 8.—H I optical depth image toward 3C 119 in a single 0.4 km s^{-1} velocity channel centered at -4.7 km s^{-1} (LSR). The gray scale represents H I optical depth from 0.35 to 0.85, and the contours represent continuum emission at 112, 374, and 748 mJy $beam^{-1}$. The angular resolution is 10 mas. The inset shows a crosscut with 2 σ error bars in optical depth along the axis indicated by the dashed line.

components are likely due to local gas (closer than 500 pc), and the H I gas at high negative velocity is probably in the Perseus arm at a distance greater than 2 kpc. At that distance, the 10 mas beam in the H I optical images corresponds to 20 AU, and the separation of 53 mas between components B and C corresponds to 100 AU.

As with 3C 147, we fitted the circular polarization spectrum toward 3C 119 to determine the line-of-sight magnetic field. A fit to the overall V and I spectra averaged over the entire source produces a 2 σ upper limit of 20 μG on the line-of-sight magnetic field.

3.3. *2352+495*

The source 2352+495 is a compact symmetric object selected from the Polatidis et al. (1995) VLBI survey. There are no published observations of H I absorption toward this source, a radio galaxy with a redshift of 0.237 and a total 21 cm continuum flux density of 2.36 Jy. The morphology of the source is a bright core with two symmetric lobes. The VLBA 21 cm continuum image of 2352+495 is shown in Figure 11, with the three bright continuum components from north to south labeled "A," "B," and "C". The angular resolution is 10 mas.

The H I optical depth spectrum toward 2352+495 is shown in Figure 12. The maximum H I optical depth is 0.25 and occurs at a velocity of 3.3 km s^{-1}, with a line width of 2.0 km s^{-1}. The H I absorption line is asymmetrical and consists of several narrow components, with the strongest line at 0.0 km s^{-1}. Figure 13 shows the optical depth image at the velocity of the maximum H I optical depth at $v = 0.0$ km s^{-1}.

Figure 14 shows the continuum image with average H I optical depth spectra toward the three bright emission components. As in Figures 5 and 10, the dashed lines indicate the VLBA data and the solid lines indicate the Gaussian profile fits. The parameters of these Gaussian profile fits are given in Table 4. Three Gaussian profiles were fitted to the spectra; however, spectral components 2 and 3 (indicated in Fig. 12) are considerably noisier than spectral component 1, and the Gaussian profile fits for those components are not well determined. These data are consistent with uniform H I absorption across the source, with no changes in H I column density exceeding 30% (1 σ).

The source 2352+495 is located at $l = 113°$ and $b = -12\overset{\circ}{.}0$. The two spectral components near 0.0 km s^{-1} are assumed to be local gas. Assuming that the thickness of the

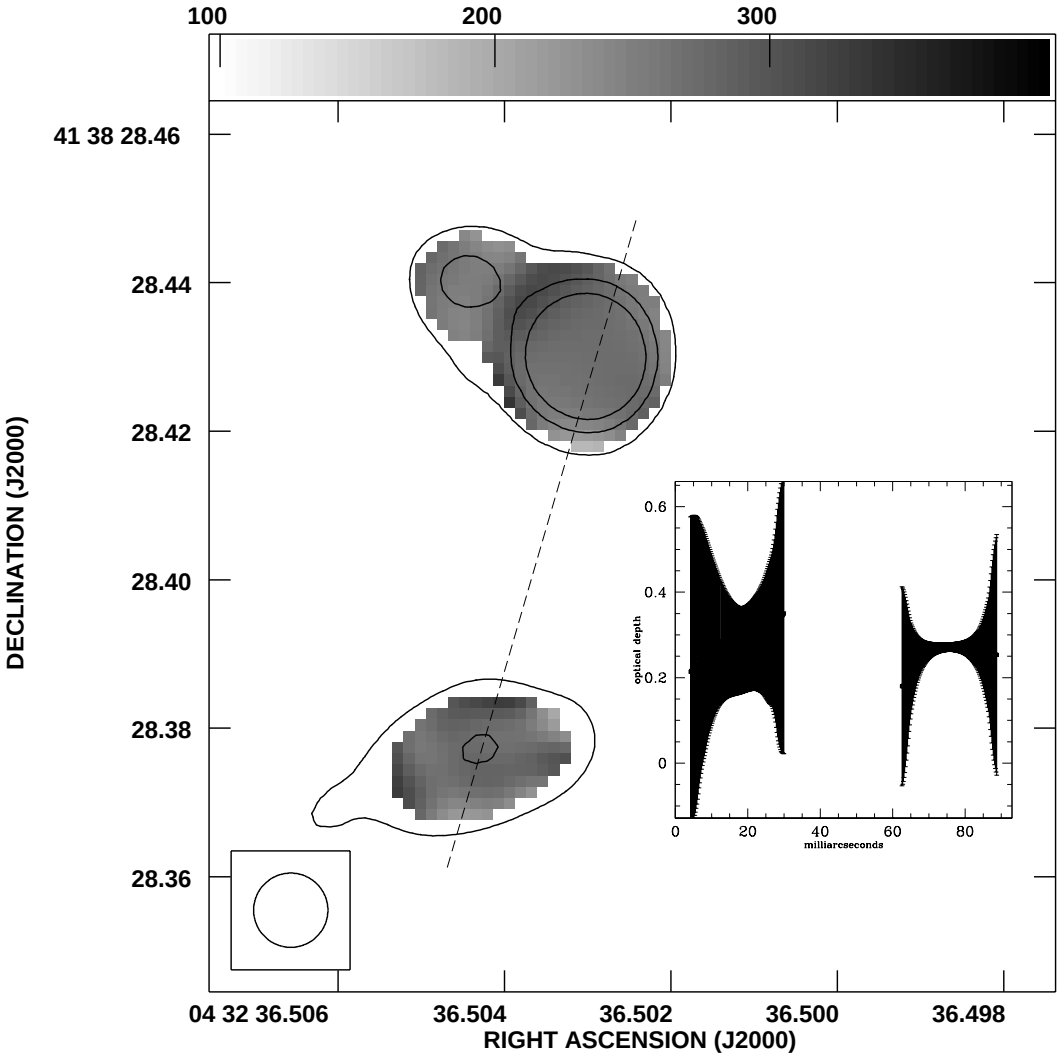


FIG. 9.—H I optical depth image toward 3C 119 in a single 0.4 km s^{-1} wide velocity channel centered at -62.6 km s^{-1} LSR velocity. The gray scale represents H I optical depth from 0.1 to 0.4, and the contours represent continuum emission at 112, 374, and 748 mJy $beam^{-1}$. The resolution of the beam is 10 mas. The inset shows a crosscut with 2 σ error bars in optical depth along the axis indicated by the dashed line.

local H I disk is less than 100 pc, H I gas along a line of sight at this Galactic latitude must lie closer than 500 pc. The resolution of the H I optical depth images of 10 mas corresponds to a linear size of 5 AU, and the separation of 50 mas between continuum components A and C corresponds to 25 AU. Assuming the rotation curve of Fich et al. (1989), the kinematic distance to the -10 km s^{-1} absorption line is 800 pc. At this distance, the 10 mas beam corresponds to a linear size of 8 AU, and the 50 mas separation between the components A and C corresponds to 40 AU.

Fits to the V and I spectra averaged over the entire source produce a 2 σ upper limit of 160 μG on the line-of-sight magnetic field.

3.4. *0831+557*

The source 0831+557 was also selected from the VLBI survey of Polatidis et al. (1995). There are no published observations of H I absorption toward this source. It has a total 21 cm continuum flux density of 8 Jy and the highest Galactic latitude of any of the sources in the sample ($b = 34.^{\circ}6$). It has very weak H I absorption in two velocity components, one at 3 km s^{-1} with a maximum H I optical depth ≈ 0.1 and the other a possible weak line near -37 km s^{-1} with a maximum H I optical depth of ≈ 0.03. The 3 km s^{-1} line has a velocity width of 2 km s^{-1}. Figure 15 shows a 21 cm continuum image of 0831+557, convolved to an angular resolution of 20 mas. There are two strong continuum components separated by about 180 mas, labeled "A" and "B" in Figure 15. Component A is significantly brighter, with a peak continuum emission of 2.9 Jy $beam^{-1}$, compared with 0.4 Jy $beam^{-1}$ peak emission for component B.

The H I optical depth spectrum toward 0831+557 is shown in Figure 16. Figure 17 shows an optical depth image toward 0831+557 at 3.9 km s^{-1}. The gray scale indicates H I optical depth from 0 to 0.2, and the contours represent weak continuum emission. The image was convolved to 20 mas to improve the signal-to-noise ratio. The inset plot shows a crosscut in optical depth along the dashed line. No significant variations in optical depth are observed between the two continuum components with a 1 σ limit in any variation of $\Delta\tau \approx 0.1$.

At a Galactic latitude of $b = +36.^{\circ}6$, a geometric upper limit to the absorbing gas is $\propto 200$ pc, assuming that the thickness of the cold H I gas is 100 pc. At that distance,

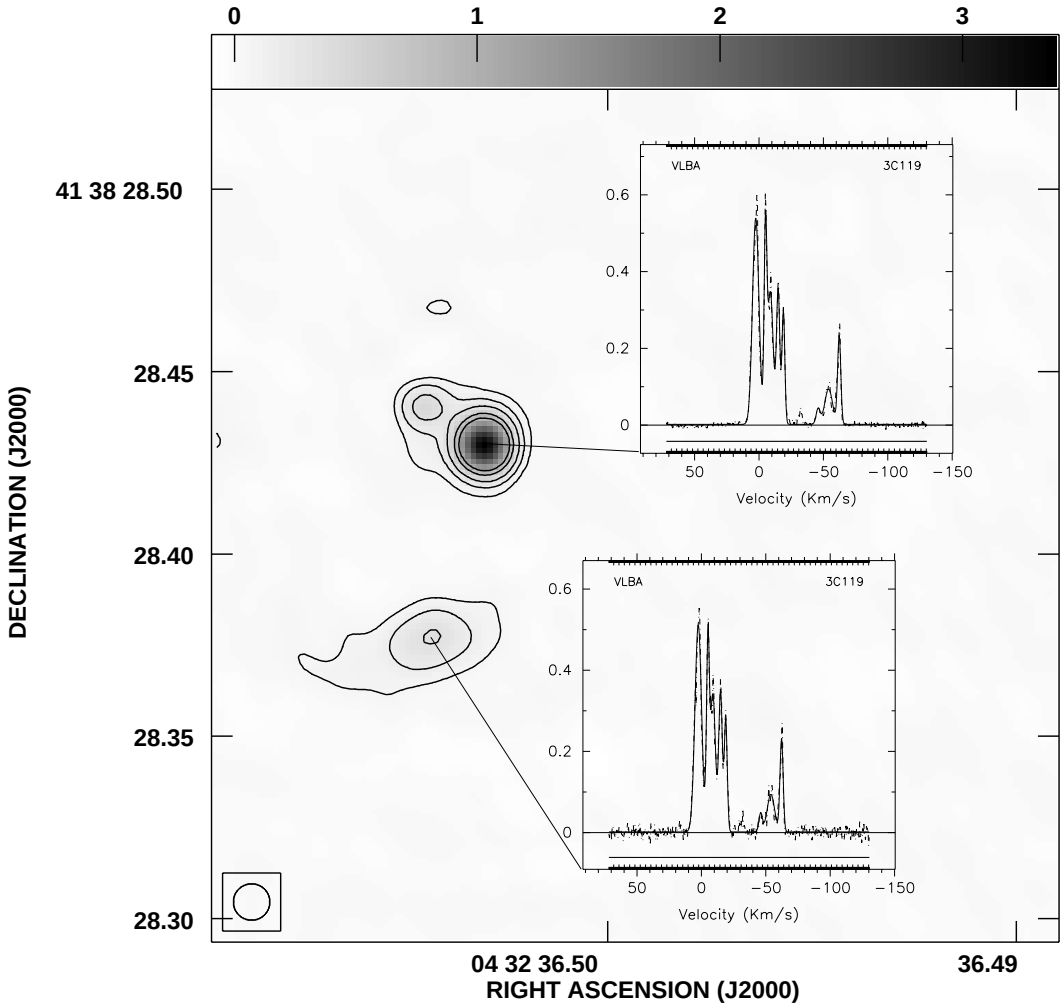


FIG. 10.—Continuum image of 3C 119. Insets show optical depth spectra averaged over the areas of brightest continuum emission. The dashed line in the insets plots shows the VLBA data, and the solid line indicates the Gaussian component fits. The parameters of the fits are given in Table 3.

TABLE 3

3C 119 H I OPTICAL DEPTH SPECTRUM FIT GAUSSIAN PARAMETERS

Spectral Component	Amplitude (Optical Depth)	Column Density[a] (10^{20} cm^{-2})	Center Velocity (km s^{-1})	Velocity Dispersion (km s^{-1})
Component B:				
1	0.54 ± 0.01	3.08 ± 0.07	2.5 ± 0.03	5.9 ± 0.07
2	0.48 ± 0.04	1.18 ± 0.1	−5.0 ± 0.04	2.5 ± 0.1
3	0.35 ± 0.03	1.71 ± 0.2	−8.8 ± 0.1	5.1 ± 0.3
4	0.35 ± 0.02	1.04 ± 0.09	−14.9 ± 0.05	3.1 ± 0.1
5	0.30 ± 0.02	0.80 ± 0.06	−19.0 ± 0.05	2.6 ± 0.1
6	0.042 ± 0.01	0.15 ± 0.06	−45.9 ± 0.3	3.7 ± 0.8
7	0.093 ± 0.01	0.64 ± 0.10	−54.1 ± 0.2	7.1 ± 0.6
8	0.23 ± 0.01	0.66 ± 0.05	−62.3 ± 0.05	2.9 ± 0.1
Component C:				
1	0.51 ± 0.01	3.0 ± 0.08	2.4 ± 0.04	6.0 ± 0.1
2	0.45 ± 0.04	1.14 ± 0.1	−5.1 ± 0.05	2.6 ± 0.1
3	0.34 ± 0.03	1.52 ± 0.2	−8.9 ± 0.1	4.6 ± 0.3
4	0.35 ± 0.03	1.09 ± 0.1	−14.9 ± 0.06	3.4 ± 0.2
5	0.28 ± 0.02	0.73 ± 0.07	−18.9 ± 0.06	2.7 ± 0.2
6	0.046 ± 0.02	0.14 ± 0.06	−46.0 ± 0.3	3.1 ± 0.7
7	0.093 ± 0.01	0.6 ± 0.1	−53.9 ± 0.2	6.8 ± 0.6
8	0.23 ± 0.02	0.64 ± 0.06	−62.3 ± 0.06	2.9 ± 0.1

[a] Assuming $T_{spin} = 50$ K.

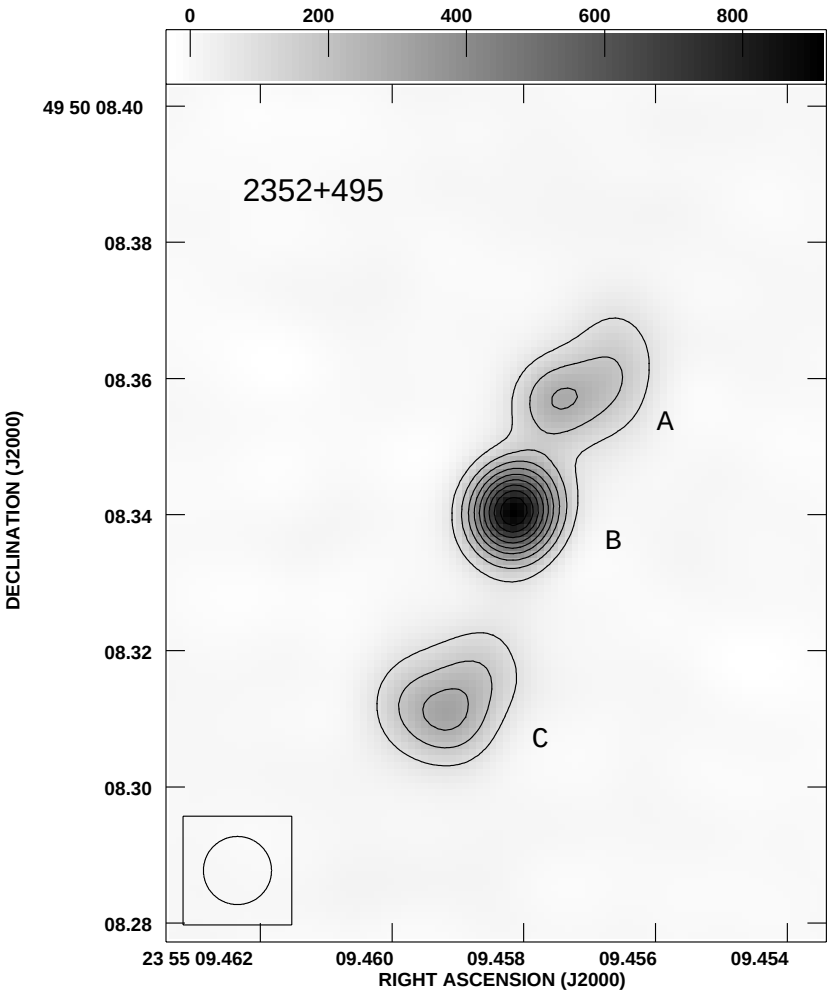


FIG. 11.—Continuum image of 2352+495 at 21 cm from the VLBA and the phased VLA. The beam has been convolved to 10 mas. The contours correspond to continuum emission at 91, 182, 273, 364, 455, 547, 638, 729, and 820 mJy beam^{-1}.

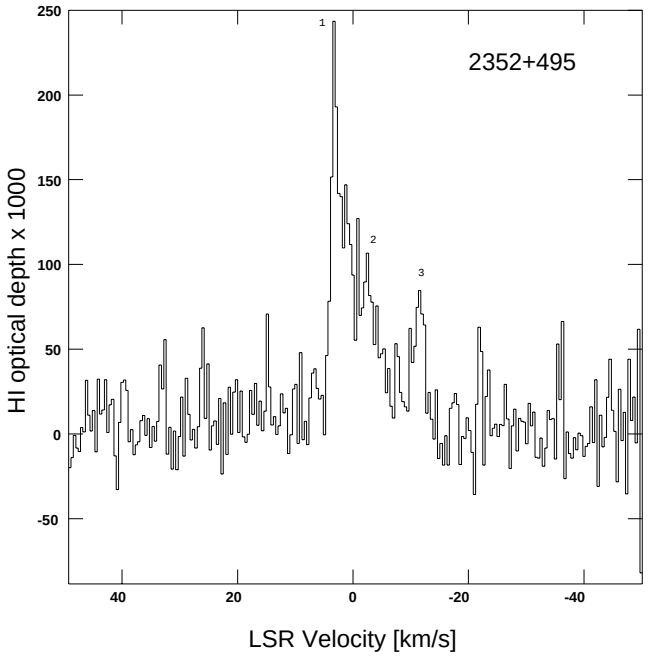


FIG. 12.—H I optical depth spectrum toward 2352+495, averaged over the source. The velocity resolution is 0.4 km s^{-1} per channel.

the angular separation of 160 mas between components A and B corresponds to a physical distance of 30 AU.

4. STRUCTURE FUNCTIONS OF THE H I OPTICAL DEPTH IMAGES

Deshpande (2000) has pointed out that the optical depth variations observed between two points on the sky represent contributions to optical depth variations on all scales, including larger scales. The optical depth difference between two points on the sky does not arise entirely from structures with this scale size. Because of the shape of the power spectrum (a "red" spectrum with enhanced fluctuations at larger scales), variations from larger structures contribute to the variations at an observed scale. This effect complicates the interpretation of the optical depth images as representing unique structures on scales of tens of AU. A proper interpretation of the actual physical scale of the structure requires knowledge of the power spectrum over larger scales. Deshpande et al. (2000) have found that the power spectrum of H I optical depth variations toward Cas A (Perseus arm feature) and in the outer arm toward Cyg A can be fitted with a power-law index of -2.75 over physical scales from 0.02 to 4 pc. For the local arm in the direction of Cyg A, the slope is shallower at -2.5. The power spectra of both Cyg A features are, however, an order

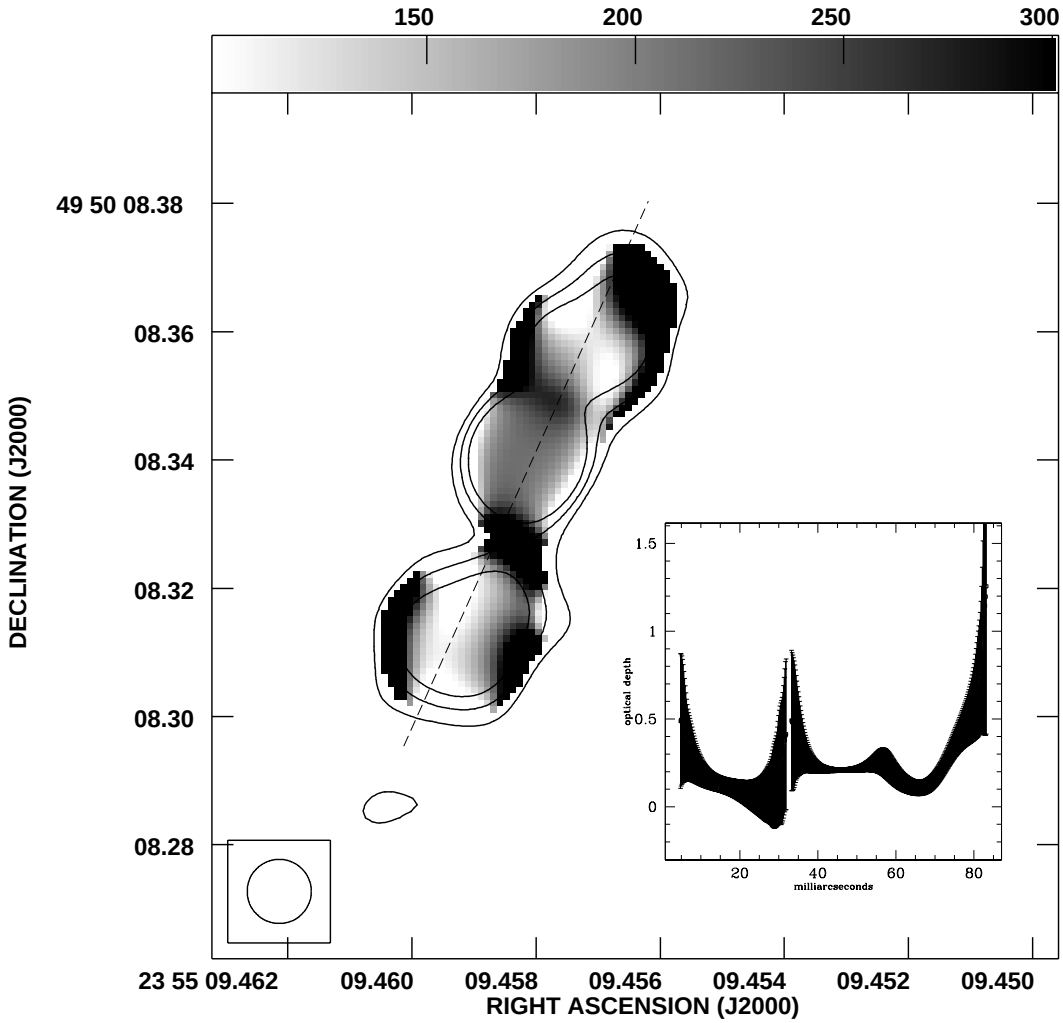


FIG. 13.—H I optical depth image toward 2352+495 in a single 0.4 km s^{-1} velocity channel centered at 3.3 km s^{-1} (LSR). The resolution of the beam is 10 mas. The gray scale corresponds to H I optical depth from 0.1 to 0.3, and the contours represent continuum emission at 18, 46, and 91 mJy $beam^{-1}$. The inset shows a crosscut with 2 σ error bars in optical depth along the axis indicated by the dashed line.

of magnitude less intense than those of the Cas A Perseus arm feature. Deshpande (2000) suggests that the power-law power spectrum with the steeper index of -2.75 can be extrapolated to size scales of 40–100 AU, a factor of almost 40 relative to the smallest scale in the measured Cas A power spectrum. Therefore, optical depth variations would be expected with root mean square values of about 0.1. This effect is shown in Figure 2 of Deshpande (2000), based on the -2.75 index for the Cas A Perseus arm data. Most of the objects in this paper and in FGDT show H I optical changes consistent with this level of variation. However, 3C 138 shows changes in excess of this prediction. For 3C 138, the changes in opacity are in the range 0.6–0.8 over a size scale of 50 mas (25 AU at a distance of 500 pc).

Deshpande (2000) also suggests that structures observed on small scales should only be observed as gradients in optical depth, because the changes on AU scales are only due to larger scale variations. Our H I optical images toward 3C 147 and 3C 138 clearly show discrete H I structures, not simply gradients. Especially convincing is the elongated two-dimensional structure in the northeast part of the image where the continuum emission of 3C 138 is very strong and the H I optical depth is therefore well determined. This part of the H I optical depth image at 0.4 km s^{-1} from FGDT is reproduced in Figure 18. These structures clearly are *not* simply gradients in optical depth.

5. DISCUSSION AND CONCLUSIONS

The optical depth variations toward 3C 147 are shown in Figure 19, a position-velocity plot for this source. The vertical axis of this plot corresponds to the axis along the source from the northwest to the southeast, as indicated in Figures 3 and 4. As can be noticed in the individual optical depth images, the optical depth variations along the axis of the source are larger in the H I absorption line near -8.3 km s^{-1} than in the line near 0.4 km s^{-1}. The opacity fluctuations far away from the absorption lines, shown in Figure 19, are a good indication of the noise in the optical depth at a given position along the axis of the source. This position-velocity plot can be compared with the position-velocity plot for 3C 138 from FGDT (their Fig. 6). Although there are obvious optical depth variations in each absorption line toward 3C 147, the striking optical depth structure changes in velocity observed toward 3C 138 are not observed in the 3C 147 position-velocity image. In the 3C 138 position-

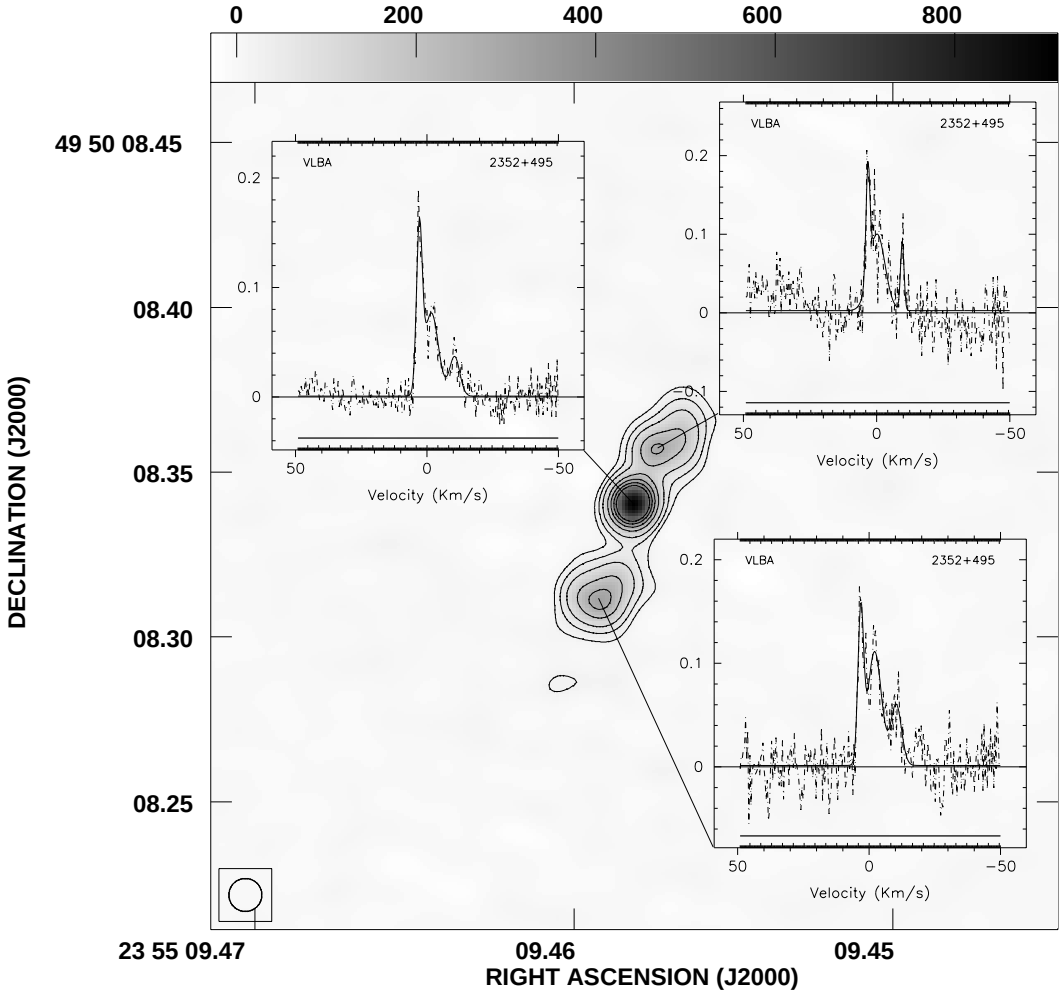


FIG. 14.—Continuum image of 2352+495. Insets show optical depth spectra averaged over the areas of brightest continuum emission. The dashed line in the insets shows the VLBA data, and the solid line indicates the Gaussian component fits. The parameters of the fits are given in Table 4.

TABLE 4

2352+495 H I OPTICAL DEPTH SPECTRUM FIT GAUSSIAN PARAMETERS

Spectral Component	Amplitude (Optical Depth)	Column Density[a] (10^{20} cm^{-2})	Center Velocity (km s^{-1})	Velocity Dispersion (km s^{-1})
Component A:				
1	0.15 ± 0.02	0.36 ± 0.07	2.9 ± 0.08	2.6 ± 0.2
2	0.076 ± 0.02	0.47 ± 0.2	-1.7 ± 0.4	6.3 ± 1.0
3	0.036 ± 0.01	0.16 ± 0.06	-10.5 ± 0.4	4.6 ± 0.9
Component B:				
1	0.14 ± 0.06	0.23 ± 0.1	3.3 ± 0.1	1.7 ± 0.4
2	0.098 ± 0.02	0.67 ± 0.2	-0.14 ± 0.6	7.0 ± 1.0
3	0.089 ± 0.04	0.13 ± 0.07	-9.6 ± 0.2	1.5 ± 0.5
Component C:				
1	0.14 ± 0.03	0.35 ± 0.1	3.2 ± 0.1	2.5 ± 0.3
2	0.11 ± 0.02	0.66 ± 0.2	-2.1 ± 0.3	6.1 ± 1.0
3	0.059 ± 0.02	0.27 ± 0.1	-10.3 ± 0.4	4.8 ± 1.1

[a] Assuming $T_{spin} = 50$ K.

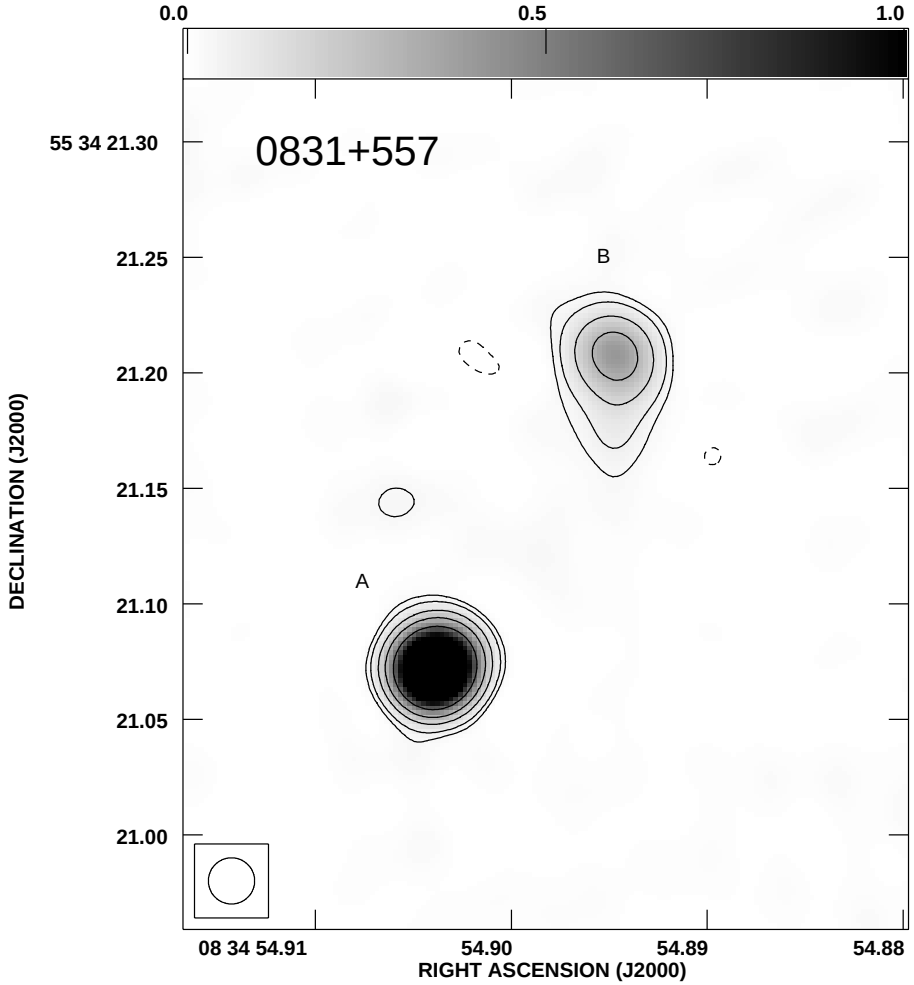


FIG. 15.—Continuum image of 0831+557 at 21 cm from the VLBA and the phased VLA. The beam has been convolved to 20 mas. The contours correspond to continuum emission at −29.2, 29.2, 58.3, 146, 292, 583, and 1460 mJy beam^{-1}.

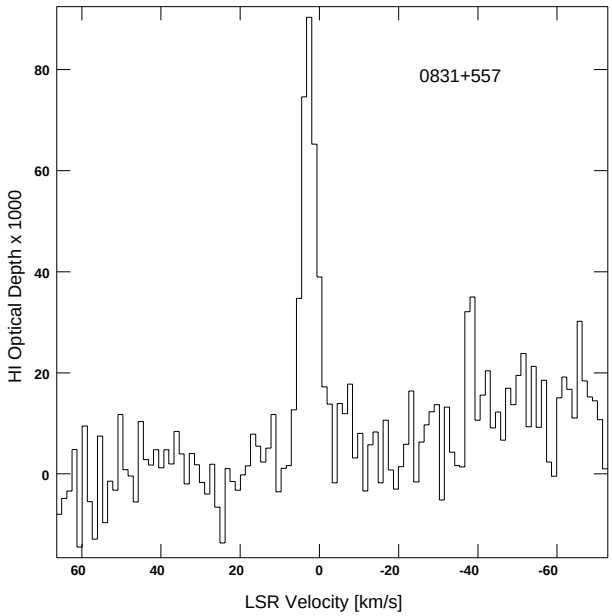


FIG. 16.—H I optical depth spectrum toward 0831+557 observed with the VLA. The velocity resolution is 1.3 km s^{-1}.

velocity plot, the velocity features that slope diagonally across are quite striking and indicate that we are observing real, three-dimensional features coherent in velocity.

The constraints on the line-of-sight magnetic field toward these sources suggest that this field is not enhanced relative to the average interstellar magnetic field of 40–100 μG. Diamond et al. (1989) determined that field strengths of 200 μG would be required to confine the small-scale structure observed toward 3C 138 relative to the pressure of the diffuse ISM. The upper limits on the line-of-sight magnetic field toward 3C 147 and 3C 138 are an order of magnitude below this value.

In conclusion, we have imaged Galactic H I in absorption toward four extragalactic continuum objects at 10 mas resolution. The −8.3 km s^{-1} H I absorption line toward the source 3C 147 shows variations of 10% to 20% in H I column density across the source (1 σ error of 5%) and variations in optical depth from about 0.82 to 1.1 (at about a 4 σ level). No significant variations are observed across the source 3C 119, either in H I optical depth to within a 1 σ error of 0.2 or in H I column density to within a 1 σ error of 10%. The source 2352+495 shows no significant H I column density variations to within a 1 σ limit of 30%. The high Galactic latitude source 0831+557 has weak H I

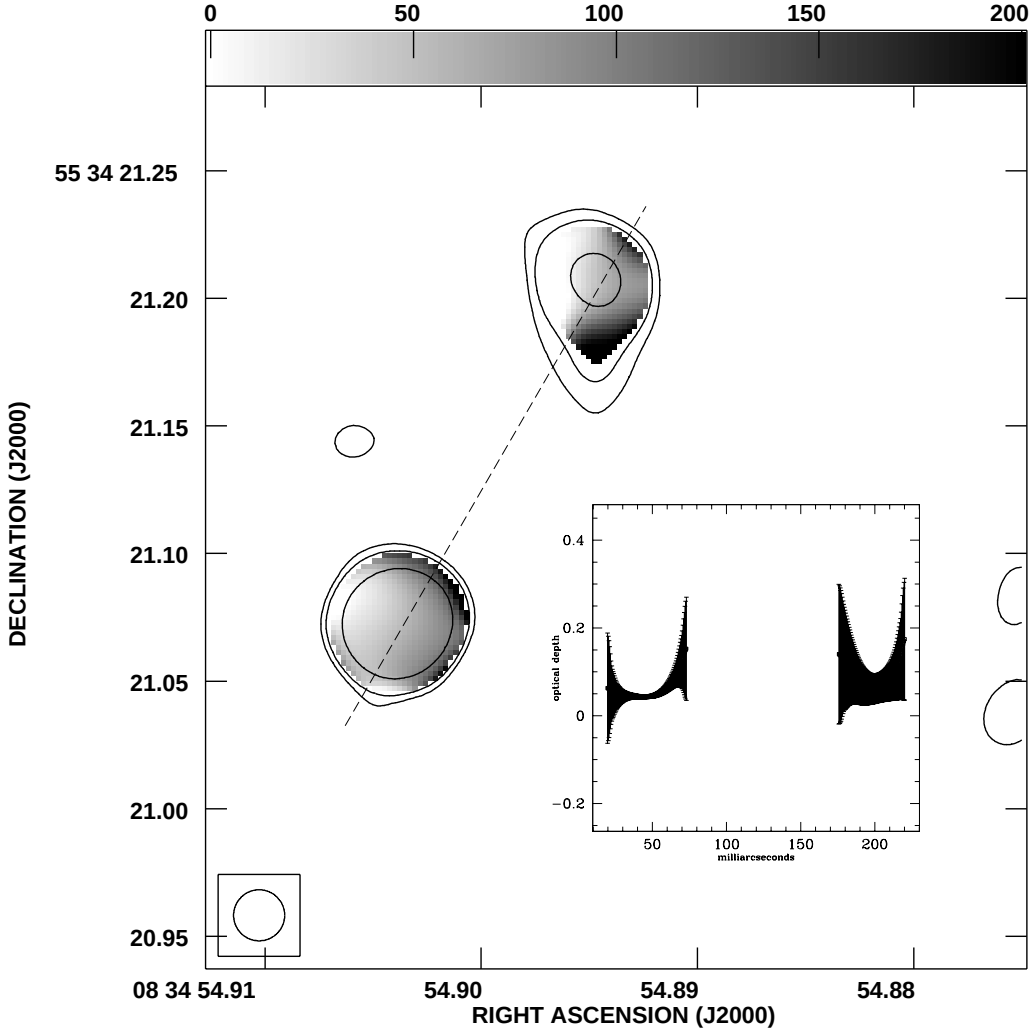


FIG. 17.—H I optical depth image toward 0831+557 in a single 0.4 km s^{-1} velocity channel centered at 3.9 km s^{-1} (LSR). The gray scale represents H I optical depth from 0.0 to 0.2, and the contours represent continuum emission at 29.2, 58.3, and 292 mJy $beam^{-1}$. The angular resolution is 20 mas. The inset shows a crosscut with 2 σ error bars in optical depth along the axis indicated by the dashed line.

absorption and shows no significant column density variations to within a 1 σ limit of 50%.

All these results are consistent with the prediction of Deshpande (2000) that optical depth variations as large as $\delta\tau \approx 0.1$ are possible on scales of hundreds of AU. However, 3C 138 is unique among the objects we have observed in showing very large H I optical depth variations of $\Delta\tau \approx 0.1$ on scales of tens of AU.

It is of considerable interest to examine the cold, neutral medium on intermediate scales between the few tens of AU probed by VLBI observations and the 0.1 pc scales probed by connected-element interferometers such as the WSRT and the VLA. The only observations published to date on angular scales between the resolution of the VLBA (about 10–500 mas) and that of the VLA (about 1″–30″) are of ISM optical lines toward binary stars (e.g., Lauroesch et al. 1998; Watson & Meyer 1996) separated by 500 to 30,000 AU. However, most of these observations are of variations in Na I column density, which may not reliably trace the H I column density. Observations of H I column density variations should be carried out on these size scales to compare the AU-scale structure with the larger scale structure. These observations could be carried out with the MERLIN array or by observing H I column density variations toward pulsars in the manner of Frail et al. (1994). The Green Bank Telescope will be an especially sensitive instrument for observing H I in absorption toward pulsars. Also, more pulsar and VLBI studies of AU-scale structure should be carried out in the southern hemisphere, outside the field of view of the VLBA. To date no observations of AU-scale structure in H I have been made from $l = 187°$ to $l = 20°$.

The VLBA and VLA are operated by the National Radio Astronomy Observatory, a facility of the National Science Foundation, operated under a cooperative agreement by Associated Universities for Research in Astronomy, Inc. We thank Ed Churchwell for helpful comments on an earlier version of this paper. We also thank A. Deshpande for providing the structure function code and assisting us with interpretation of the structure functions of the optical depth images.

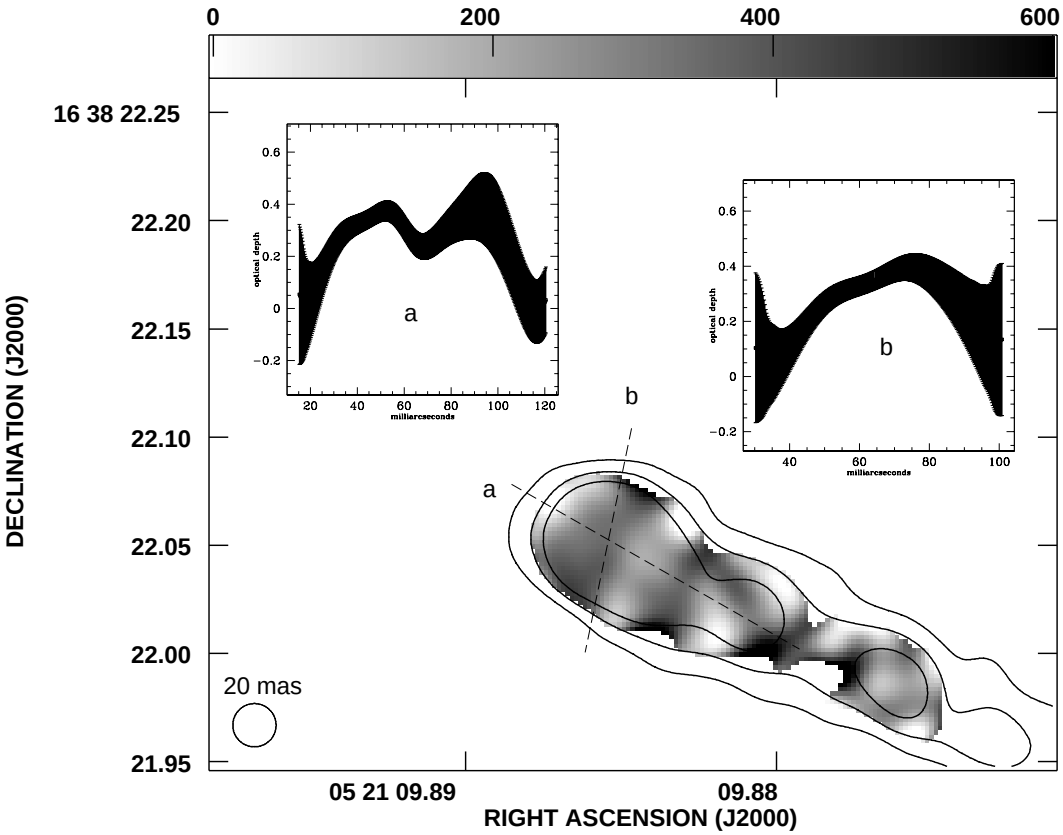


FIG. 18.—Section of the H I optical depth image at 0.4 km s^{-1} of 3C 138, taken from FGDT. Two cross sections in optical depth are shown with 2σ errors (*insets*).

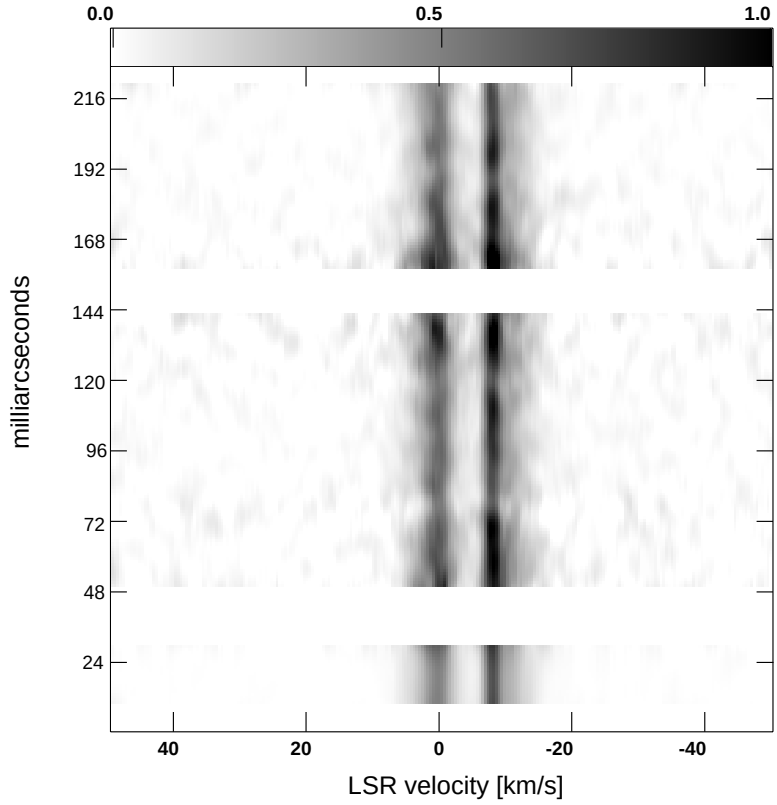


FIG. 19.—Position-velocity plot for 3C 147 along the axis of the source indicated by the dashed line in Figs. 3 and 4. The horizontal axis indicates LSR velocity, and the vertical axis indicates angular distance from the upper northwest corner of the source. The gray scale indicates H I optical depth from 0.0 to 1.0. Variation in optical depth can be observed as a change in the gray scale along a vertical line in this plot. More prominent variations in optical depth are observed along the source axis at the -8.3 km s^{-1} line than at the 0.4 km s^{-1} line.

REFERENCES

Armstrong, J. W., Rickett, B. J., & Spangler, S. R. 1995, ApJ, 443, 209
Crovisier, J., & Dickey, J. M. 1983, A&A, 122, 282
Davis, R. J., Diamond, P. J., & Goss, W. M. 1996, MNRAS, 283, 1105 (DDG)
Deshpande, A. A. 2000, MNRAS, 317, 199
Deshpande, A. A., Dwarakanath, K. S., & Goss, W. M. 2000 ApJ, 543, 227
Dewdney, P. E., & Lozinskaya, T. A. 1994, AJ, 108, 2212
Diamond, P. J., Goss, W. M., Romney, J. D., Booth, R. S., Kalberla, P. M. W., & Mebold, U. 1989, ApJ, 347, 302
Dieter, N. H., Welch, W. J., & Romney, J. D. 1976, ApJ, 206, L113
Faison, M. D., Goss, W. M., Diamond, P. J., & Taylor, G. B. 1998, AJ, 116, 2916 (FGDT)
Fich, M., Blitz, L., & Stark, A. A. 1989, ApJ, 342, 272
Frail, D. A., Weisberg, J. M., Cordes, J. M., & Mathers C. 1994, ApJ, 436, 144
Green, D. A. 1993, MNRAS, 262, 327
Heiles, C. 1997, ApJ, 481, 193
Kalberla, P. M. W., Schwarz, U. J., & Goss, W. M. 1985, A&A, 144, 27
Lauroesch, J. T., Meyer, D. M., Watson, J. K., & Blades, J. C. 1998, ApJ, 507, L89
Marscher, A. P., Moore, E. M., & Bania, T. M. 1993, ApJ, 419, L101
Mebold, U., Winnberg, A., Kalberla, P. M. W., & Goss, W. M. 1981, A&AS, 46, 389
Moore, E. M., & Marscher, A. P. 1995, ApJ, 452, 671
Nan, R., Gabuzda, D. C., Kameno, S., Schilizzi, R. T., & Inoue, M. 1999, A&A, 344, 402
Nan, R., Schilizzi, R. T., van Breugel, W. J. M., Fanti, C., Fanti, R., Muxlow, T. W. B., & Spencer, R. E. 1991, A&A, 245, 449
Polatidis, A. G., Wilkinson, P. N., Xu W., Readhead, A. C. S., Pearson, T. J., Taylor, G. B., & Vermeulen, R. C. 1995, ApJS, 98, 1
Radhakrishnan, V., Brooks, J. W., Goss, W. M., Murray, J. D., & Schwarz, U. J. 1972, ApJS, 24, 1
Sault R. J., Teuben P. J., & Wright M. C. H. 1995, in ASP Conf. Ser. 77, Astronomical Data Analysis Software and Systems IV, ed. R. Shaw, H. E. Payne, & J. J. E. Hayes (San Francisco: ASP), 433
Watson, J. K., & Meyer, D. M. 1996, ApJ, 473, L127